Thomson scattering system at the Tokyo electron beam ion trap

Hideharu Kuramoto,[a] Tohru Kinugawa, Hirofumi Watanabe, Chikashi Yamada,[b] and Shunsuke Ohtani[b]
Cold Trapped Ions Project, ICORP, Japan Science and Technology Corporation (JST), Axis Chofu 3F, 1-40-2 Fuda, Chofu, Tokyo 182-0024, Japan

Ichihiro Yamada
National Institute for Fusion Science, Toki, Gifu 509-5254, Japan

Frederick John Currell
Queen's University, Belfast BT7, 1NN, Northern Ireland

(Received 7 August 2001; accepted for publication 22 October 2001)

A Thomson scattering system has been installed at the Tokyo electron beam ion trap for probing characteristics of the electron beam. A YVO_4 green laser beam was injected antiparallel to the electron beam. The image of the Thomson scattering light from the electron beam has been observed using a charged-coupled device camera. By using a combination of interference filters, the spectral distribution of the Thomson scattering light has been measured. The Doppler shift observed for the scattered light is consistent with the beam energy. The beam radius dependence was investigated as a function of the beam energy, the beam current, and the magnetic field at the trap region. The variation of the measured beam radius against the beam current and the magnetic field were similar to those in Herrmann's prediction. The beam radius as a function of the beam energy was also similar to Herrmann's prediction but seemed to become larger at low energy. © *2002 American Institute of Physics.* [DOI: 10.1063/1.1427418]

I. INTRODUCTION

The electron beam ion trap (EBIT) was developed at Lawrence Livermore National Laboratory[1] for spectroscopic studies of highly charged ions HCIs and was based on the electron beam ion source concepts[2] but with a shorter ion trap length to limit plasmalike instabilities. More recently a high-energy EBIT with some design differences has been constructed in Tokyo, being dubbed the Tokyo EBIT.[3] With this device, a systematic study for x-ray spectroscopy[4] of HCIs has been performed. In this measurement, the radiation source size is defined by the electron beam radius and can be used directly for dispersive spectroscopy without an entrance slit,[5] so the size of the beam is one of the limiting parameters to the resolution. It is, therefore, important to know the electron beam diameter accurately. Furthermore, in order to measure absolute cross sections for electron–ion interactions such as the ionization cross section of ions by electron impact, using the rate of onset of ion production,[6] it is necessary to know the current density of the electron beam, which can be obtained from the measurement of the radial intensity profile at the ion-trap region.

The theoretical electron beam diameter in the trap is described by Herrmann's theory,[7] in which the electron beam radius in a magnetic field B is given by

$$r_h = r_b \sqrt{\frac{1}{2} + \frac{1}{2}\sqrt{1 + 4\left(\frac{8kTr_c^2}{m\eta^2 r_b^4 B^2} + \frac{B_c^2 r_c^4}{B^2 r_b^4}\right)}}, \tag{1}$$

where r_h is the effective beam radius, defined as the radius containing 80% of the beam current, kT is the temperature of the electron gun cathode, r_c the cathode radius, B_c the magnetic field at the cathode surface, m the electron mass, η the electron's charge to mass ratio, and r_b is the beam radius for Brillouin flow given in μm by

$$r_b \approx \frac{150}{B}\frac{\sqrt{I_e}}{(E_e)^{1/4}}, \tag{2}$$

where I_e is the beam current in amperes, B the magnetic field at the trap region in tesla, and E_e is the beam energy in keV. For any EBIT, the first term in round brackets is always much greater than unity. Hence, the equation can be considerably simplified by neglecting the small constants that are added to this term, under the square-root signs. When the magnetic field at the cathode is zero, the beam radius is its minimum value. Enforcing this condition leads to further simplification. Combining Eqs. (1) and (2) and converting to suitable units then gives the minimum beam radius (i.e., optimum bucking coil tuning) to be

$$r_h[\mu\mathrm{m}] \approx 260\sqrt{\frac{r_c[\mathrm{cm}]}{B[\mathrm{T}]}}\sqrt{kT[\mathrm{eV}]}. \tag{3}$$

Knapp *et al.* measured the radial size of the electron beam from a pinhole image of x-ray radiation from super-EBIT.[8] When imaging photons from short-lived x-ray transitions, ambiguity exists because the feature really imaged is the electron-ion overlap. Cold ions can predominantly lie inside the electron beam, leading to an underestimate of the beam radius. Furthermore, there are angular alignment difficulties associated with this form of measure-

[a]Electronic mail: kuramoto@hci.jst.go.jp
[b]Also at the University of Electro-Communications, Chofu, Tokyo 182-8585, Japan.

ment since a slit typically 1-cm long but about 10-μm wide, placed close to the electron beam in a high magnification configuration. Hence, even a small misalignment of the slit axis relative to the electron beam axis could lead to significant errors in the measured beam radius. For observations of visible light emitted by the trapped ions, the radiation image does not show directly the beam size because some of the transitions are long enough lived that the ions can leave the electron beam before emitting light. In case of the ions having long lifetimes, the radiation image can show the ion cloud distribution.[9]

In the early 1960s, soon after the invention of the laser, Fiocco and Thompson[10] observed weak scattering signals of optical radiation at an angle $\theta=65°$ from a 2 keV, 75 mA electron beam using a ruby laser (20 J, 800 μs). Recently, 30 keV x rays generated by 90° Thomson scattering of a femtosecond, near infrared, terawatt laser in the forward direction from a bunched 50 MeV electron beam was observed[11] to measure transverse and longitudinal density distributions of the beam with subpicosecond resolution. This technique can be expected to become important for diagnosing electron bunches in the accelerators.

In this paper, we introduce our efforts to diagnose the electron beam characteristics in the EBIT device by using Thomson scattering with a 5 W, cw green laser.

II. EXPERIMENTAL SETUP

The Tokyo-EBIT[12–14] consists of three parts, namely an electron gun, a cryostat region including drift tubes, and an electron collector. Electrons emitted from the cathode with a radius of 1.5 mm are accelerated upwards by the potential difference between the electron gun and the drift tubes, while being magnetically compressed by a pair of superconducting Helmholtz coils. In the center drift tube, there are eight slots (10-mmlong×2-mmwide) arranged parallel to the electron beam, one of which is used for the present observation. After passing through the drift tube assembly, the electron beam reaches the collector region where the beam diverges, is decelerated, and collected. HCIs can be produced inside the center drift tube by successive ionization process through interactions with electrons, and trapped radially by the space charge of the electron beam and axially by an electrostatic potential well which is created along a set of three collinear drift tube electrodes.

The experimental setup for the Thomson scattering measurement is shown schematically in Fig. 1. The laser source is a diode-pumped, frequency-doubled Nd: Vanadate ($Nd:YVO_4$) laser (COHERENT Verdi) that provides single-frequency green (532 nm) light at an output power level of about 5 W (maximum 6 W). The 3 mm laser light is focused to about 1 mm in diameter by a lens ($f=2500$ mm) and counterinjected into the drift tube region. The intensity profile of the laser beam is almost uniform. The polarization of the incident light is perpendicular to the axis of the electron beam as shown in Fig. 1. Radiation scattered through 90° by the electron beam is collected by a lens system. After passing through the polarizer and filters, the scattered light is detected by a liquid-nitrogen-cooled CCD camera (Princeton

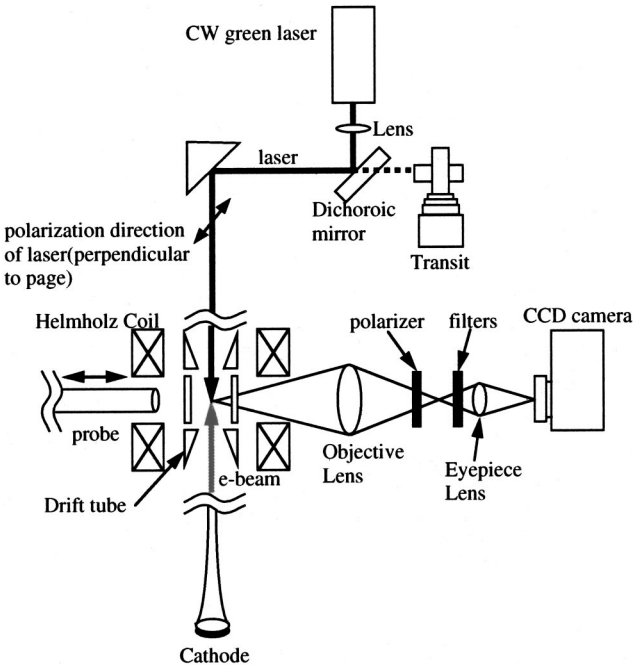

FIG. 1. Schematical view of the experimental setup for Thomson scattering measurement.

Instruments, LN/CCD-1100PB/VISAR) which has a 1100 ×330 pixel array with 24 μm pixel pitch. A 100-mm diameter objective lens with a focal length of 153.8 mm is located 347 mm from the electron beam. As shown in Fig. 1, an eyepiece lens is used at front of the CCD camera to make a magnification of the image to be about 10. The position of the camera is adjusted along the optical axis by using a He-Ne laser and also by observing visible emissions from trapped ions in the EBIT.

Alignment of the laser axis is carefully performed to obtain true signals with good signal-to-noise (S/N) ratios in this experiment. A finely adjustable dichroic mirror is used for the alignment; by simultaneous observation of the back-reflected laser beam and light due to thermal emission from the cathode seen through the transit. The tilt angle of this mirror is carefully adjusted so that the laser and cathode images are concentric. After this overlap adjustment, the laser beam is considered to hit the cathode because the e-beam current increases slightly due to enhanced thermionic emission from the cathode through absorption of the laser power.

Three filters are in use for measuring the Thomson scattering signal, namely two color glasses (HOYA B-390 and MELLES GRIOT KG-3) and an interference filter (SIGMA KOKI DIF-50S-BLE) with a 95% transmittance for a wide range of the wavelengths 390–470 nm. The B-390 glass with a transmission of 6×10^{-3}% at 530 nm is used for eliminating the stray laser light scattered from the wall of the drift tube and the KG-3 glass for rejecting infrared photons from the cathode. A DIF-50S-BLE is used for transmitting the Doppler-shifted light (i.e. the Thomson scattering signal). In order to observe the spectral distribution for the scattered light by the electron beam, a set of seven narrow-band interference filters with different center wavelengths are used.

A polarizer is also used in front of the CCD camera. True signals due to Thomson scattering are detected by using the polarizer aligned to the polarization axis of the incident laser light, while background signals are measured by changing the polarization axis of the polarizer to be perpendicular to that of the incident light. In order to obtain good statistics with high S/N ratios, the difference between true and background signals is determined for every measurement. Noise signals due to cosmic rays are automatically removed by a software procedure which looks for erroneously high isolated readings in the CCD readout.

In order to calibrate the size of the Thomson scattering image, a probe as shown in Fig. 1 is used. This prove moves from the outside of the drift tube to the center. The real size of the electron beam is determined by comparing with the image at the CCD camera of the probe head (1-mm diameter) located at the center, which is illuminated by visible light.

III. RESULTS AND DISCUSSION

A. Thomson scattering measurements

Figure 2 shows the scattered light images observed by the CCD camera. These measurements were made with a 15 keV, 100 mA electron beam. In order to confirm that Thomson scattering signals were observed, two sets of experiments were performed. In the first set of the experiments, we observed the scattered light signals from the trap region with and without electron beam. A typical result is shown in Fig. 2(a). In the second set of experiments, as shown in Fig. 2(b), we measured the intensity of the scattered light with the polarizer parallel (0°) and perpendicular (90°) to the polarization of the laser. For these observations, the laser power used was 2 W and exposure time for the CCD camera was 150 s. A hill-shaped potential was applied to the three drift tubes (i.e., DT2 is much more positive than DT1 or DT3, so ions are quickly accelerated out of the trap) during the measurement to eliminate visible photons from trapped ions. As seen on the CCD images in Fig. 2(a) and 2(b), clear peaks due to Thomson scattering are observed at around pixel 550. The bumps on both sides of the main peak, which are observed both at the laser beam on and off, are due to reflection on the wall of the central drift tube of unpolarized infrared photons from the cathode. In Fig. 2(b) the dotted line is considered to be a contribution of the stray/background light. True signals due to Thomson scattering can be obtained by subtraction of the dotted line from the solid line distribution, as is shown in Fig. 2(c). By integrating the total photons detected at around pixel 550, the count rate due to the Thomson scattering is estimated to be 8.8 photons/s.

The total number (N) of scattered photons is calculated using the Thomson scattering cross section ($d\sigma/d\Omega \sim 3.97 \times 10^{-26}\,\mathrm{cm}^2/\mathrm{str}$):

$$N = \frac{d\sigma}{d\Omega}\Delta\Omega L \frac{J}{\pi r^2 h\nu}\frac{I}{ev}, \tag{4}$$

where $\Delta\Omega$ is the observation solid angle, L is the observation length of the interaction between the laser and the electron beam, J the laser power, r the radius of the laser beam, h Planck's constant, ν the frequency of the laser, I the electron beam current, e the elementary charge, and v is the velocity of the electrons ($v = 7.27 \times 10^7\,[\mathrm{m/s}]$ at 15 keV). For the present experimental conditions, N is estimated to be 7.8 photons/s, which is in good agreement with the observed count rate.

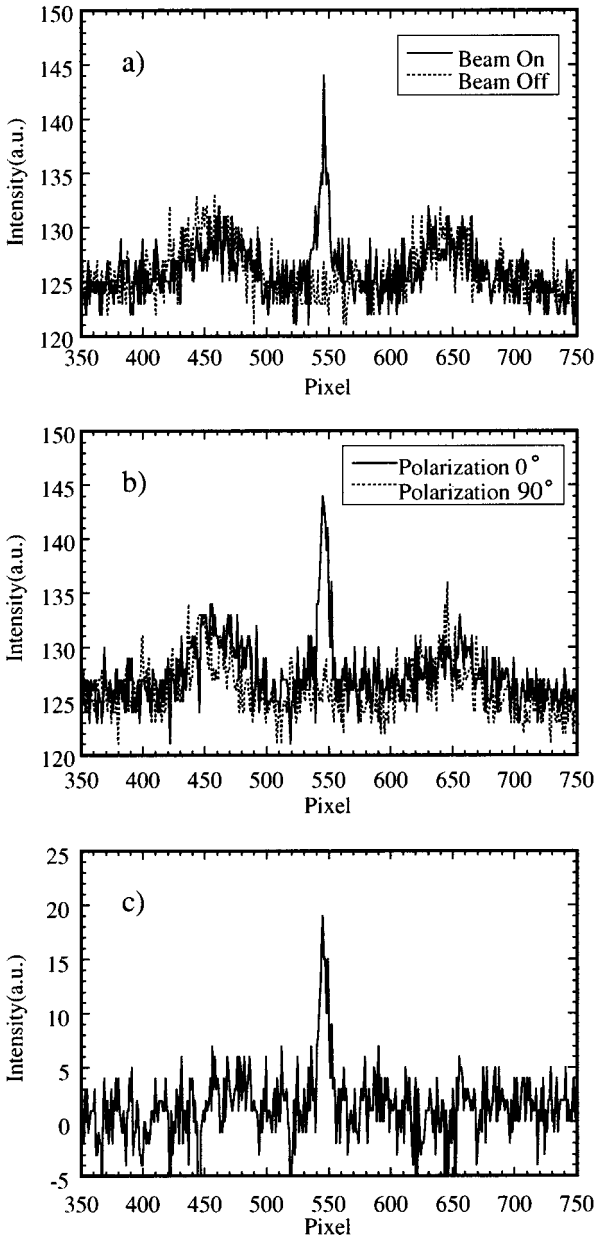

FIG. 2. (a) Signal with/without electron beam. (b) Signal with parallel/perpendicular polarization. In each figure, the broad bumps on both sides of the main peak are reflected light from the drift tube. (c) The true signal obtained by subtraction of the dotted line from the solid line in (b).

B. Thomson scattering spectrum measurements

Under our experimental condition, of head-on laser-electron collisions observed at right angles, the scattered light is Doppler shifted, depending on the electron velocity. In other words, we can determine the velocity of the electron beam through measurements of the wavelength for the scattered light. In Fig. 3, spectral distributions measured for the scattered light are shown at two different acceleration voltages for electrons: 15 and 23 kV. Scattered intensity at each

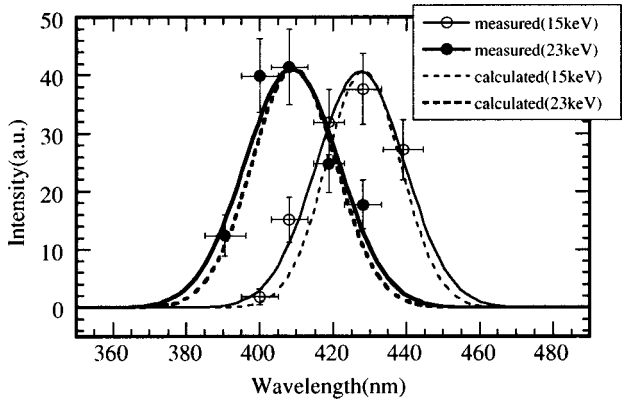

FIG. 3. Spectral distribution of the Thomson scattered light measured by using the set of interference filters. Solid lines are Gaussian fitting profiles and broken lines are the calculated distributions.

wavelength has been estimated by considering the wavelength-dependent transmittance of the respective filter used. The solid lines show Gaussian fits for each spectral distribution. The broadening of the Doppler-shifted profile is due to two phenomena, the transverse temperature of the electron beam and the solid angle of observation. The broken lines in Fig. 3 are Gaussian with widths determined by the quadrature sum of the widths of these two broadening mechanisms.

The heights of these Gaussians were normalized to the measurements. The central wavelengths were calculated from the relativistic Doppler shift and the width was calculated from the quadrature sum of the solid angle of this system (about 13°) and transverse velocity of electron beam. Herrmann showed that the magnitude of the transverse velocity is inversely proportional to the radius of the cathode images formed at various locations along the electron beam axis.[7] In other words, the product of beam area and transverse electron energy are constant at these locations. We can thus estimate transverse electron energy from the temperature of the cathode of the electron gun (=0.1 eV) and the areal compression ratio of the beam (from a radius of about 1.5 mm at the cathode to about 0.03 mm in the trap) to be about 250 eV.

Assuming that, in the present experimental arrangement, both electron and laser beams have no divergence and also the observation angle of scattered photons is just 90°, the Doppler-shifted wavelength is given by

$$\lambda_D = \frac{\lambda_{\text{laser}}}{1+\nu/c}, \tag{5}$$

where λ_{laser} is the incident laser wavelength, ν the velocity of electrons, and c the speed of the light. Then the electron beam energy (E_{beam}) is expressed in keV by

$$E_{\text{beam}} = \left\{ 15.95 \times \left(\frac{\lambda_{\text{laser}}}{\lambda_D} - 1 \right) \right\}^2. \tag{6}$$

Using this equation, the measured energies of electron beam are calculated to be 15.2 and 23.1 keV with an accuracy of about 3% at accelerating voltages of 15 and 23 kV, respectively. Hence, the observed Doppler shift is consistent with the expected beam energy.

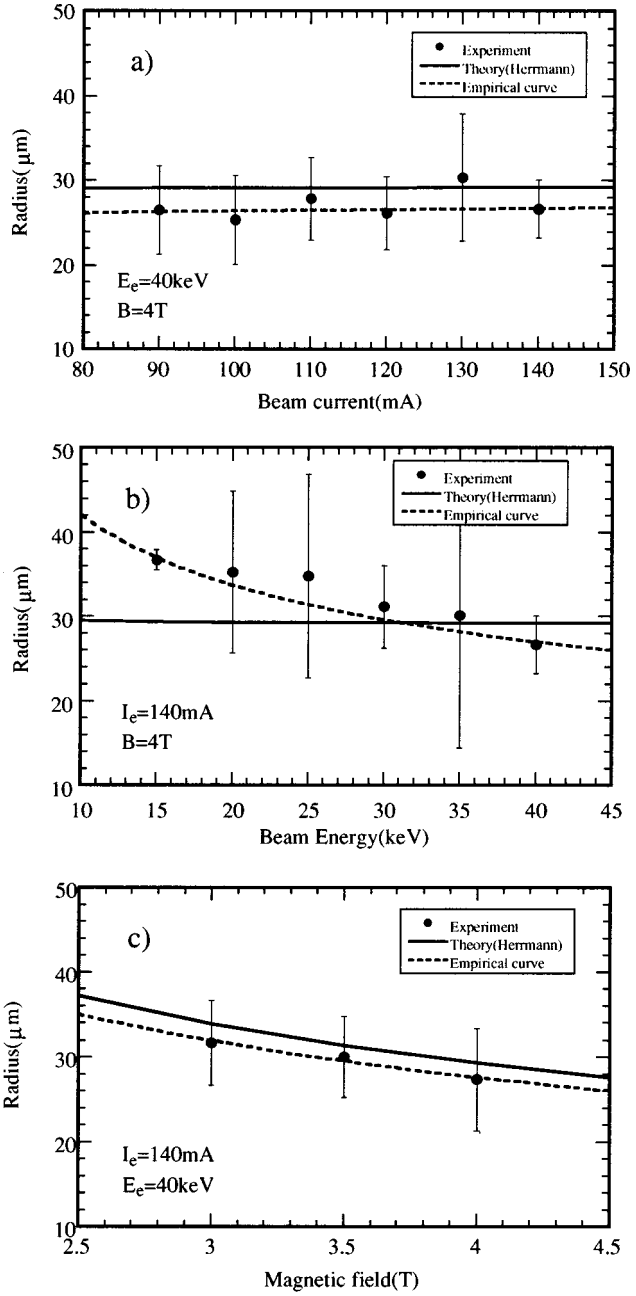

FIG. 4. Measured beam radius as a function of operating parameters, beam current, energy, and magnetic-field applied at the trap.

C. Beam radius measurements

After a pioneering work for determination of the electron beam radius using an x-ray pinhole camera in the super-EBIT by Knap *et al.* in 1993,[8] Utter *et al.*[15] made systematic observations of the electron beam's position and diameter as a function of operating parameters including beam energy and current, tuning of the steering magnets, adjustment of the bucking coil, and superconducting magnet current. They observed the beam radius remaining almost unchanged between 35 and 37 μm, with beam energies ranging from 17.9 to 67.9 keV when the beam current was kept constant at 90 mA. On the other hand, the beam radius increased remarkably with the current from 90 to 230 mA at the same energy of 136 keV.

The properties of the electron beam might vary from device to device as dictated by the design and the operation of each individual EBIT. Furthermore, Thomson scattering has some advantages as a diagnostic as discussed above. Therefore, we have measured the beam radius as a function of various operating parameters. The result is shown in Fig. 4(a) for the beam radius as a function of the beam current. The beam energy E_e was kept constant at 40 keV and the magnetic field at the trap B was 4 T. In this figure, circles show the measured values and the solid line indicates the calculation from Herrmann's theory using Eq. (1). The measurement seems to agree well with the calculation. The radius is almost constant as the beam current I_e is varied as is expected from Eq. (3). Hence, the electron density increases linearly with I_e. The E_e dependence on the radius is shown in Fig. 4(b). In this measurement, I_e and B were kept constant at 140 mA and 4 T, respectively. The error bars at the beam acceleration energies of 20, 25, and 35 keV are large, coming from poor counting statistics due to short data accumulations, while the error bar at 15 keV is smaller because the data accumulation procedure was repeated ten times. The experimental data at 30 and 40 keV are each the sum of five separate accumulations. As shown in this figure, the experimental values at lower energies seem to be slightly larger than the calculation.

In the EBIT operation, a strong magnetic field B compresses the electron beam. The beam radius, therefore, should become smaller with increasing B as dictated by Eq. (3). Figure 4(c) shows the behavior of the beam compression with B, where E_e and I_e were kept constant at 40 keV and 140 mA, respectively. The measured radius is also in good agreement with the theory.

In these results, the beam radius seems to become larger with decreasing energy, that is, it is seemed that the beam radius shows stronger dependence on the beam energy than Herrmann's theory, although the experimental values are scattered in the present observation. We obtained an empirical fitting curve for the energy dependence of the beam radius, which is proportional to $E_e^{-0.5}$, as shown by a broken line in Fig. 4(b). This empirical formula reproduces well the measured values for the current- and magnetic-field dependencies of the beam radius, as shown in Fig. 4(a) and 4(c).

The discrepancy between the measurements and the theory is not clearly understood. In order to understand characteristics of the electron beam in the EBIT, it is necessary to accumulate more data for various beam energies, and also to investigate other parameter dependencies such as kT and B_c.

In these measurements for the electron beam characteristics, we have observed the position of the beam. Almost no shift in the position of the beam was seen with the various values for E_e, I_e, and B reported here. The position of the beam, however, was observed to shift with a change of the magnetic field at the cathode, B_c, which is controlled by the current of the bucking coil located around the electron gun region. In the present experiment, the current of the bucking coil was adjusted so that B_c is approximately zero.

ACKNOWLEDGMENTS

The authors are grateful for helpful discussions with other members in the Tokyo-EBIT group. This work was performed in the International Co-Operative Research Project (ICORP) of the Japan Science and Technology corporation. One of us (F.J.C.) also gratefully acknowledges the Royal Society for travel funding used to facilitate this collaborative research.

[1] M. A. Levine *et al.*, Phys. Scr. **T22**, 157 (1988).
[2] E. D. Donets and V. P. Orsyannikov, Sov. Phys. JETP **53**, 466 (1981).
[3] H. Kuramoto *et al.*, Rev. Sci. Instrum. **71**, 687 (2000).
[4] N. Nakamura, D. Kato, and S. Ohtani, Phys. Rev. A **61**, 052510 (2000).
[5] P. Beirsdorfer *et al.*, Rev. Sci. Instrum. **61**, 2338 (1990).
[6] E. Sokell *et al.*, Phys. Scr. **T80**, 289 (1999).
[7] G. Herrmann, J. Appl. Phys. **29**, 127 (1958).
[8] D. A. Knapp *et al.*, Nucl. Instrum. Methods Phys. Res. A **334**, 305 (1993).
[9] J. V. Porto, I. Kink, and J. D. Gillaspy, Rev. Sci. Instrum. **71**, 3050 (2000).
[10] G. Fiocco and E. Thompson, Phys. Rev. Lett. **10**, 89 (1963).
[11] W. P. Leemans *et al.*, IEEE J. Quantum Electron. **33**, 1925 (1997).
[12] F. J. Currell *et al.*, J. Phys. Soc. Jpn. **65**, 3186 (1996).
[13] H. Watanabe *et al.*, J. Phys. Soc. Jpn. **66**, 3795 (1997).
[14] N. Nakamura *et al.*, Rev. Sci. Instrum. **69**, 694 (1998).
[15] S. B. Utter, P. Beiersdorfer, J. R. Crespo Lopez-Urrutia, and K. Widmann, Nucl. Instrum. Methods Phys. Res. A **428**, 276 (1999).